tvst

Article

A Robust Microbead Occlusion Model of Glaucoma for the Common Marmoset

Sandeep Kumar[1], Alexandra Benavente-Perez[1], Reynolds Ablordeppey[1], Carol Lin[1], Suresh Viswanathan[1], Abram Akopian[1], and Stewart A. Bloomfield[1]

[1] Department of Biological and Vision Sciences, State University of New York College of Optometry, New York, NY, USA

Correspondence: Stewart A. Bloomfield, Department of Biological and Vision Sciences, SUNY College of Optometry, 33 West 42nd Street, New York, NY 10036, USA. e-mail: sbloomfield@sunyopt.edu

Received: July 20, 2021
Accepted: December 20, 2021
Published: January 12, 2022

Keywords: glaucoma; animal model; marmoset

Citation: Kumar S, Benavente-Perez A, Ablordeppey R, Lin C, Viswanathan S, Akopian A, Bloomfield SA. A robust microbead occlusion model of glaucoma for the common marmoset. Transl Vis Sci Technol. 2022;11(1):14, https://doi.org/10.1167/tvst.11.1.14

Purpose: To establish a robust experimental model of glaucoma in the common marmoset (*Callithrix jacchus*), a New World primate, using an intracameral microbead injection technique.

Methods: Elevated intraocular pressure (IOP) was induced by an injection of polystyrene microbeads. Morphologic changes in the retina and optic nerve of glaucomatous eyes were assessed and electroretinogram (ERG) recordings were performed to evaluate functional changes.

Results: Microbead injections induced a sustained IOP elevation for at least 10 weeks in a reproducible manner. At the end of the 10-week experimental period, there was significant loss of retinal ganglion cells (RGCs) in all quadrants and eccentricities, although it was more prominent in the mid-peripheral and peripheral regions. This was consistent with a thinning of the Retinal nerve fiber layer (RNFL) seen in spectral domain optical coherence tomography scans. Surviving RGCs showed marked changes in morphology, including somatic shrinkage and dendritic atrophy. Retinas also showed significant gliosis. The amplitude of the ERG photopic negative response, with subsequent a- and b-wave changes, was reduced in glaucomatous eyes. The optic nerve of glaucomatous eyes showed expanded cupping, disorganization of the astrocytic matrix, axonal loss, and gliosis.

Conclusions: We developed a robust and reproducible model of glaucoma in the marmoset. The model exhibits both structural and functional alterations of retina and optic nerve characteristic of glaucoma in humans and animal models.

Translational Relevance: The glaucoma model in the marmoset described here forms a robust method to study the disease etiology, progression, and potential therapies in a nonhuman primate, allowing for more effective translation of animal data to humans.

Introduction

Glaucoma, a major cause of vision impairment worldwide, is often associated with elevated intraocular pressure (IOP) and characterized by progressive degeneration of retinal ganglion cells (RGCs) and more distal retinal neurons.[1,2] Studies using animal models of glaucoma have made significant contributions to our understanding of the mechanisms underlying the disease etiology and progression. Most animal studies of glaucoma pathophysiology and development have been conducted in rodents due to their practicality, cost-effectiveness, and availability of genetic lines. However, the anatomy of the retina, optic nerve, and central visual pathways in rodents differs markedly from those in humans.[3–5] Therefore, to validate results gleaned from rodent models of glaucoma and translate them to human treatments, studies have turned to glaucoma models in nonhuman primates (NHPs).[6,7] Over the past few decades, experimental NHP models of glaucoma have been developed based mainly on laser photocoagulation of the perilimbal region,[8–11] cauterization of episcleral veins,[12] hypertonic saline injection into the episcleral veins,[13] and intracameral injection of microbeads.[14–17]

While studies of these various NHP glaucoma models have furthered our understanding of the

disease process, their use has encountered significant downsides. These include impracticalities such as ethical issues involving large NHP use and care, high animal costs, variability of results, and the inability to genetically manipulate animals. Moreover, NHP models often rely on complex surgical interventions to elevate IOP that can cause ocular inflammation and flattening of the anterior chamber, thereby resulting in unwanted variability in the magnitude and duration of IOP changes. In this regard, the microbead occlusion model, first developed for the mouse,[18] has proven advantageous in its ability to produce consistent, sustained elevations of IOP without complex surgical intervention and the resulting risk of serious intraocular inflammation.[14–16,19]

The common marmoset (*Callithrix jacchus*), a small-bodied New World monkey, is considered an excellent model for vision research in that they are relatively easy to handle, breed well in captivity, share visual acuity and foveal specializations to other NHPs and humans, and have been successfully used for transgenic studies.[20–22] In fact, the common marmoset is listed as a key animal model for gene editing in the National Institutes of Health (NIH) BRAIN Initiative (RFA-DA-21-006) supported by the National Eye Institute (NEI). The marmoset thus represents a desirable subject for creation of an NHP glaucoma model. To the best of our knowledge, only one study has established a marmoset ocular hypertension model using laser trabeculoplasty.[10] However, the authors reported that the extent and duration of elevated IOP levels after laser treatment were inconsistent across treated eyes.

Here, we describe a new, robust, and reproducible microbead occlusion model of glaucoma in the common marmoset. Our model shows many structural and functional abnormalities phenotypic of glaucoma,[2,23] including a sustained elevation of IOP for at least a 10-week period, reduction of electroretinogram (ERG) waveform amplitude, significant remodeling of RGC dendritic structure followed by cell loss, Retinal nerve fiber layer (RNFL) thinning, structural changes and axonal loss in the optic nerve, and reactive gliosis in both retina and optic nerve.

Methods

Experimental Animals

Experiments were performed on common marmosets (*Callithrix jacchus*) of both sexes with initial ages 12 to 14 months. Animals were kept under a 12:12-hour ambient light cycle and fed ad libitum. All animal procedures followed the NIH Guide for the Care and Use of Laboratory Animals, as well as the ARVO Statement for the Use of Animals in Ophthalmic and Vision Research, and were approved by the Institutional Animal Care and Use Committee (IACUC) at the State University of New York College of Optometry.

IOP Elevation by Microbead Injection

Experimental glaucoma was initiated by IOP elevation induced with an intracameral injection of 10-µm diameter polystyrene microbeads (Invitrogen, Carlsbad, CA, USA) into the anterior chamber, as previously described in a mouse model of glaucoma.[18,19] Animals were anesthetized (alphaxalone, 15 mg/kg body weight, intramuscular [IM]) and placed on a warm heating pad. Body temperature, respiration rate, heart rate, and peripheral capillary oxygen saturation (SpO_2) were monitored during the procedure. Injections were performed unilaterally with a 25-µL microbead suspension (~14.4×10^7 microbeads) using a 30-gauge needle connected to a microsyringe. The cornea was gently punctured using a 30-gauge needle prior to intracameral injections. The microbead injection was repeated at week 4, which maintained elevated IOP for at least 10 weeks. An equivalent volume of phosphate-buffered saline (PBS) was injected into the contralateral eyes at weeks 0 and 4 to serve as a sham control. Animals were closely monitored after injections for eye inflammation, anterior chamber flares, or scleral leakage, which were not seen in the four experimental animals in this study. Animals were less active for a day or two after injection but returned to normal social behavior afterward. For tissue collection at study termination, animals were anesthetized (alphaxalone, 15 mg/kg body weight, IM) prior to euthanization (Beuthanasia-D, 0.5 mL/100 g, intracardiac (IC)). Enucleations were then performed, and retinas were isolated and assessed histologically for structural and cellular changes.

IOP Measurements

IOP measurements were made using a veterinary tonometer Tono-Pen Avia Vet (Reichert Technologies; Dan Scott and Associates, Westerville, OH, USA). Measurements were performed 10 minutes after anesthetizing the animals with an intramuscular injection of alphaxalone (15 mg/kg body weight) and topical application of 0.5% proparacaine. Subsequent measurements were performed weekly between 10 AM and 12 PM to minimize the effect of diurnal IOP variation. Five to six measurements were obtained per eye and averaged.

Spectral Domain Optical Coherence Tomography Imaging

Spectral domain optical coherence tomography (SD-OCT) was performed using the Bioptigen SD-OCT (Leica Microsystems, Inc., Buffalo Grove, IL, USA) at baseline prior to bead injection and at the end of treatment prior to tissue collection. The SD-OCT provided high-resolution cross-sectional retinal scans and fundus images of the marmoset retina using rectangular volume retinal scans (12×12 mm^2, 700 A-scans/B-scans and 70 B-scans and 5 frames/B-scans)[24,25] while the animals were anesthetized (alfaxalone 15 mg/kg body weight, IM) and wore custom-made rigid contact lenses of +0.00 diopters (D) to prevent tear film evaporation.

The scan segmentation was performed at the same location pre- and posttreatment. The software we used for SD-OCT imaging did not provide automated calculation of Bruch's membrane opening (BMO) or minimum rim width. We therefore calculated the cup size manually using Bruch's membrane as a reference point from which the rim parameters of the optic nerve head were computed. The BMO represents the boundary of the optic disc. The minimum distance between BMO and the inner limiting membrane was taken as a geometrically accurate estimate of the rim width, called BMO-MRW, which has been found to have higher sensitivity than peripapillary RNFL thickness measures in glaucoma.[26]

To assess RNFL thickness changes in microbead-injected eyes as compared to controls, the SD-OCT scans were automatically segmented using Iowa Reference Algorithms (Retinal Image Analysis La; Iowa Institute of Biomedical Imaging, Iowa City, IA, USA). Measurements were centered at the fovea and in expanding concentric quadrants for 2.5 mm. Data were plotted as color, territorial heatmaps using MATLAB software (MathWorks, Natick, MA, USA).

Immunohistochemistry

The immunohistochemical methods have been described previously for the mouse retina.[19] Briefly, the eyecups were fixed with 4% paraformaldehyde in 0.1 M PBS, pH 7.4, for 30 minutes at room temperature and washed extensively with 0.1 M PBS. Retinal whole mounts were dissected and then blocked in 0.1 M PBS containing 10% normal donkey serum (NDS), 1% bovine serum albumin (BSA), and 0.5% Triton X-100 for 1 hour. Tissues were then incubated with primary antibodies diluted in 0.1 M PBS containing 3% NDS, 1% BSA, and 0.1% Triton X-100 for 48 hours at 4°C. After an extensive washing in 0.1 M PBS, tissues were incubated for 2 to 4 hours in secondary antibodies. Tissues were then mounted in Vectashield media with DAPI (H-1200; Vector Labs, Burlingame, CA, USA). The primary antibodies used were anti-GFAP (1:1000, Neuromics, Edina, MN, USA) for astrocyte and Müller cell gliosis, anti-Brn3a for RGC somata (1:500; Santa Cruz Biotechnology, Dallas, TX, USA), and anti-SMI32 (1:2000; Covance, Princeton, NJ, USA) for RGC dendrites and axons. The secondary antibodies used were donkey anti-rabbit/mouse/goat conjugated with Alexa 488/594/633 (1:200; Life Technologies, Carlsbad, CA, USA). Images of immunolabeled tissues were taken with an Olympus FV1200 MPE confocal microscope (Olympus, Tokyo, Japan) with 20× or 40× (oil immersion) objectives. High-resolution (1024×1024 pixels) Z-stack images were taken using step sizes of 0.7 to 2.0 µm, compiled to a single plane and analyzed quantitatively with Fluoview FV1000 and/or ImageJ (NIH) software. The brightness and contrast of micrographs were adjusted using Photoshop CS6 (Adobe, San Jose, CA, USA).

Optic Nerve Preparation and Immunostaining

Globes attached with optic nerves were isolated and then dissected ~1 mm anterior to the optic nerve head. The posterior part of the eye with optic nerve was fixed with 4% paraformaldehyde in 0.1 M PBS, pH 7.4, for 30 minutes at room temperature. Tissues were then cryoprotected sequentially in 10%, 20%, and 30% sucrose and embedded in tissue freezing medium (Electron Microscopy Science, Hatfield, PA, USA), after which 10-µm-thick frozen sections were cut through the lamina cribrosa region. Cross sections were blocked and immunostained for anti-GFAP and anti-SMI32 primary antibodies as described above and mounted on a glass slide with Vectashield medium containing the nuclear stain DAPI.

Assessment of Retinal Injury and Neuronal Loss

The detailed methods to evaluate neuronal loss and morphologic changes have been described previously.[19] Confocal images of retinal whole mounts were obtained at 40× magnification and measurements were made using Fluoview software (Olympus). To assess structural changes in RGC dendrites and axons caused by high IOP, we used ImageJ analysis software (NIH, Bethesda, MD, USA) to quantify the number of pixels with immunolabels above background in images obtained from retinal whole mounts. The number

of pixels positive for a particular marker was then divided by the total number of pixels in the image and presented as a percentage of covered area. These measures were independent of differences in the intensity of label within or across retinas as the analysis was performed with grayscale thresholding. RGCs were counted separately in at least four retinal areas of 300 × 300 µm, located in the central, mid-peripheral, and peripheral regions within the superior, inferior, nasal, and temporal retinal quadrants. The values for eccentricities were taken as distances from the fovea pit according to previous studies,[27,28] as central (1.5–2 mm), mid-peripheral (2–4 mm), and peripheral (>4 mm). Cell counts for each eccentricity and quadrant were converted to cells/mm^2 and averaged across four retinas for each control and experimental condition.

Using ImageJ software, the dendritic length of SMI32-positive RGCs was computed as the length of the longest branch from the insertion point of the primary dendrite at the soma to the ending of the terminal dendrite. The dendritic perimeter was also computed with ImageJ by forming a box around the dendritic terminal endings and summing the length of the perimeter segments. All data were imported into Sigmaplot software (Systat Software, San Jose, CA, USA) and histograms were constructed.

Electrophysiology

Animals were anesthetized with a combination of acepromazine (0.25 mg/kg body weight, IM), ketamine (25 mg/kg body weight, IM), and dexmedetomidine (0.5 mg/kg body weight, IM) and placed on a warm heating pad. This combination of drugs was found to provide adequate anesthesia without attenuation of ERG waves. ERG recordings were performed and the a-wave, b-wave, and the photopic negative response (PhNR) were analyzed.[29] Body temperature, respirations, SpO_2, and pulse rate were monitored every 15 minutes during recording. Responses were averaged over 5 to 50 stimuli. For all recordings, the largest Fourier component at 60 Hz was removed digitally to simulate a notch filter with no phase distortion having a bandwidth <0.02 Hz. Due to IACUC-imposed limitations of one protocol under anesthesia per week and the allowable length of a protocol under anesthesia, ERG recordings could be made from only one eye in a single session.

Statistics

Data are presented as mean ± SEM from at least three independent experiments. Sample sizes were calculated from a power analysis using pilot data obtained in our laboratory under the following assumptions: $\alpha = 0.05$ and power = 0.8. Eyes that showed signs of inflammation or cataract, which were limited to early pilot experiments, were excluded from analysis. Samples were allocated to their experimental groups, and therefore there was no randomization. To compare the numbers between two experimental groups, we used a two-tailed Student's t-test. Values of $P < 0.05$ were considered statistically significant.

Results

Sustained IOP Elevation Following Microbead Injection

We induced experimental glaucoma in the marmoset by unilateral microbead injections. Following the initial injection at week 0, we observed a rise in the IOP at week 2, which declined through weeks 3 and 4. Therefore, a second microbead injection was performed at week 4, which resulted in a significantly elevated IOP that was sustained over the 10-week experimental period, averaging 38.8 ± 2.6 mm Hg as compared to the control average of 20.3 ± 0.7 mm Hg ($P < 0.01$, $n = 4$ animals) (Fig. 1A). This elevation of the IOP was consistent across all four animals over the 10-week period.

The Effects of IOP Elevation on the ERG

To study the effects of elevated IOP on retinal function, we compared the photopic flash ERG recorded under control conditions and at 8 and 10 weeks after the initial microbead injection (Fig. 1B). Due to IACUC-imposed limitations to the number and duration of protocols per week under anesthesia, ERG recordings from individual animals were made from microbead-injected eyes but were not possible from the contralateral control eyes. The control ERG waveform we used was therefore the average of recordings made from 15 control animals averaging 11 months of age, closely matching that of the four experimental animals. The control response showed a gradual increase in a-wave, b-wave, and PhNR amplitudes with increasing flash intensity (average maximum amplitude [at 26 Phot cd-s/m^2]: PhNR = 41 ± 14 µV; a-wave = 50 ± 12 µV; b-wave = 100 ± 31 µV). Relative to these control responses, we observed a selective reduction in the PhNR at 8 weeks when the a- and b-waves showed relatively normal amplitudes in all four experimental animals (average maximum amplitude: PhNR = 32 ± 5 µV; a-wave = 52 ±12 µV; b-wave = 90 ± 27 µV). At 10 weeks, the PhNR amplitude continued

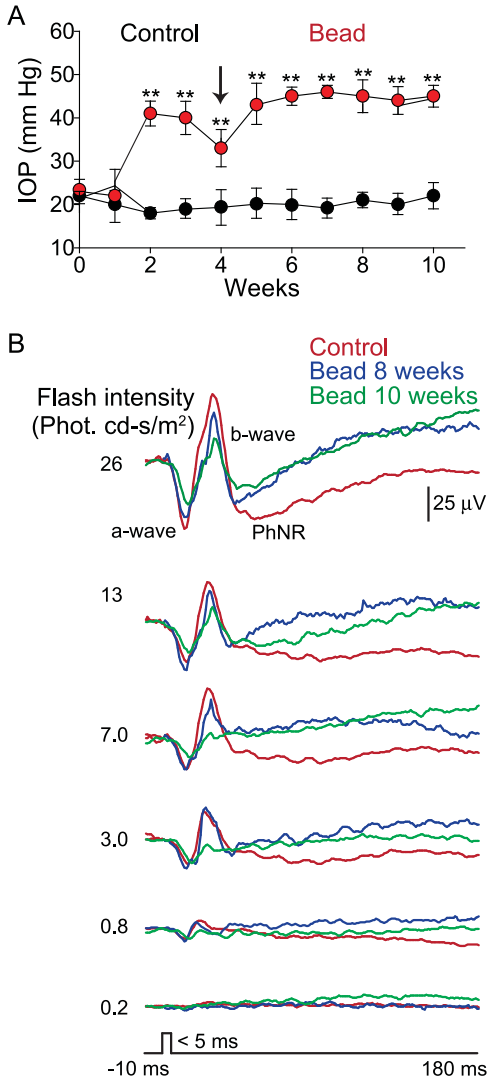

Figure 1. Effects of IOP elevation generated by microbead injection on the flash ERG. (A) Data showing sustained IOP elevation for a 10-week period, beginning at 2 weeks after an initial microbead injection followed by a second injection at week 4 (arrow) compared to control (sham injection of PBS) eyes. $^{**}P < 0.01$. (B) Full-field photopic flash ERG recordings from an individual marmoset in response to increasing stimulus strengths at 8 weeks (*blue*) and 10 weeks (*green*) after initial microbead injection. This is compared to the control ERG recordings, which is an average of the responses from 15 age-matched control animals (*red*). The PhNR in microbead-injected eyes was markedly reduced from control levels beginning at 8 weeks, whereas significant reduction of the a- and b-wave amplitudes was not seen until 10 weeks.

to decrease, but we now observed a significant reduction in amplitude and delay in the peak response times of the a- and b-waves, compared to control values in all four experimental animals (average maximum amplitude: PhNR = 18 ± 6 µV; a-wave = 19 ± 8 µV; b-wave = 33 ± 15 µV).

Given the cellular origin of the PhNR,[29,30] its selective reduction at 8 weeks after bead injection is suggestive of early damage limited to RGCs. The subsequent changes seen in the a- and b-waves, with origins in photoreceptors and bipolar cells, respectively, suggest a pattern of late damage that encompasses neurons in more distal layers,[31,32] consistent with previous reports.[33–35]

Morphologic Changes of RGCs Following IOP Elevation

We next assessed the loss of RGCs in glaucomatous eyes by comparative histochemical analysis of retinas from control eyes and those obtained 10 weeks after the initial microbead injection. We also investigated changes in glial cell activity, termed *reactive gliosis*, which results in an upregulation of GFAP expression in astrocytes and retinal Müller cells.[36] Retinal whole mounts from control and glaucomatous eyes were double immunostained with anti-Brn3a to identify RGCs[37] and with anti-GFAP to assess gliosis. Measurements were made from the central, mid-peripheral, and peripheral regions within the superior, inferior, nasal, and temporal retinal quadrants.

In control eyes, we observed a steep decline in the density of RGCs from center to peripheral retina, 7200 ± 800 cell/mm^2 to 1055 ± 30 cells/mm^2, consistent with earlier findings in primate retina[28,38] (Figs. 2A, 2B, 2C, 2G). However, we found no significant difference in RGC counts in the four retinal quadrants at the same retinal eccentricity (i.e., central, mid-peripheral, or peripheral regions). At 10 weeks after the initial microbead injection, we found a marked decrease in the density of Brn3a-positive RGCs at all three eccentricities, but cell loss was more prominent within the mid-peripheral and peripheral regions (Figs. 2D, 2E, 2F, 2G). Glaucomatous eyes showed a ~31% ($P < 0.05$, $n = 4$ eyes) reduction in RGC density in central retinas, whereas the number of RGCs within the mid-periphery and periphery was reduced by ~47% ($P < 0.001$, $n = 4$ eyes) and ~60% ($P < 0.0001$, $n = 4$ eyes), respectively (Fig. 2G).

We observed a relatively low expression of GFAP immunolabeling in control marmoset eyes and a modest increase in labeling from peripheral to central retina (Figs. 2A, 2B, 2C, 2H). At 10 weeks after the initial microbead injection, we found a significant increase in GFAP expression, indicating prominent gliosis in the retina. Interestingly, the increase in GFAP was essentially the same, 440% to 450%, within the central, mid-peripheral, and peripheral regions ($P < 0.0001$, $n = 4$ eyes) (Fig. 2H).

In glaucoma, RGCs undergo a pattern of degeneration that includes early remodeling of the dendritic

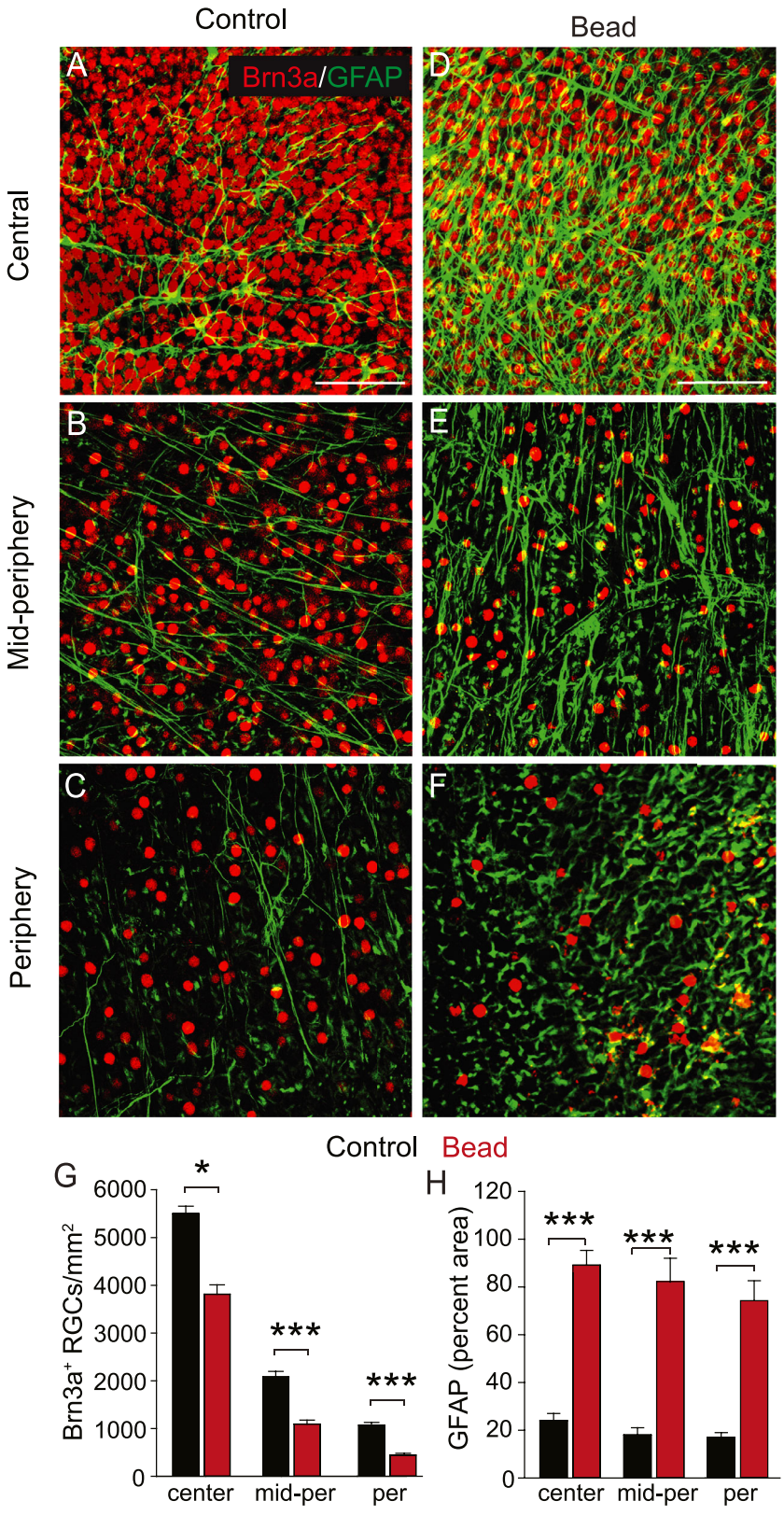

Figure 2. Territorial RGC loss and gliosis in glaucomatous marmoset eyes. (A–C) Confocal images from the central, mid-peripheral, and peripheral regions of control retinas immunostained with anti-Brn3a and anti-GFAP to visualize RGCs and astrocytes, respectively. *Scale bar*: 50 µm. (D–F) Confocal images of retinas at 10 weeks after the initial microbead injection. Conventions are the same as in panels A–C. *Scale bar*: 50 µm. (G) Histogram showing the number of RGCs at different eccentricities in control retinas and in retinas at 10 weeks after initial

→

←
microbead injection. (H) Histogram quantifying GFAP expression in control retinas and retinas at 10 weeks after initial microbead injection. Projection of three images, z = 1 µm for all images. For all histograms, $n = 3$ control retinas and $n = 4$ microbead-injected retinas. Data are presented as mean ± SEM. *$P < 0.05$, ***$P < 0.001$.

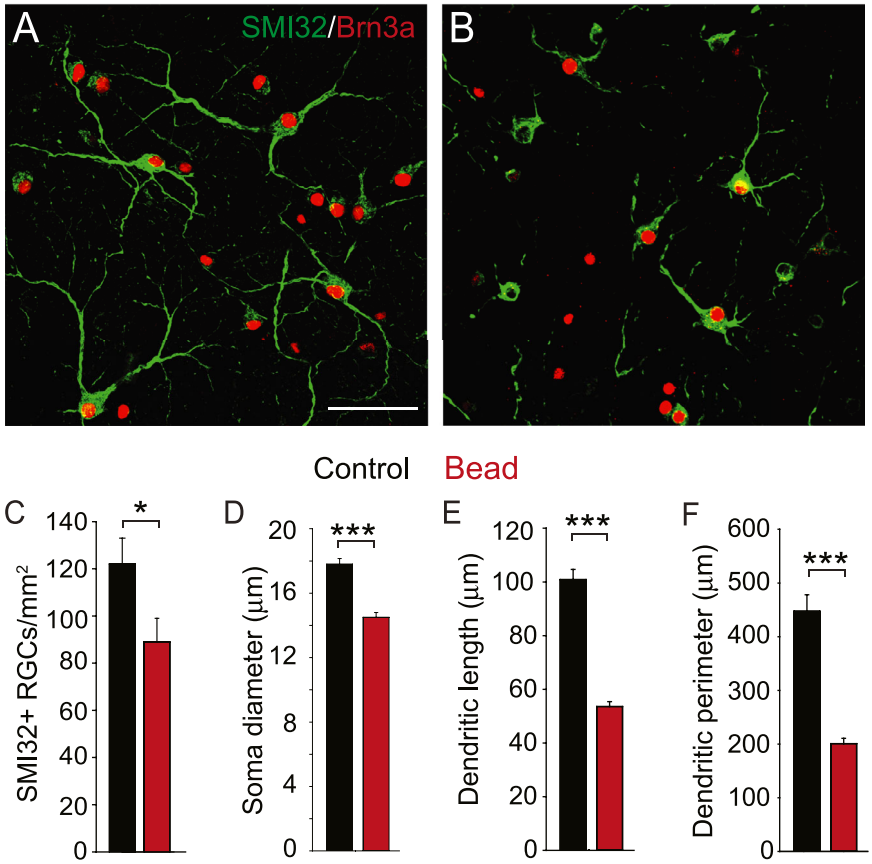

Figure 3. Effect of elevated IOP on dendritic morphology of presumed α-RGCs. (A) Confocal image of α-RGCs in peripheral retina whose dendrites are labeled with anti-SMI32 and somata labeled with anti-Brn3a. *Scale bar*: 50 µm. (B) At 10 weeks after the initial microbead injection, there is a marked loss of α-RGCs, with surviving cells showing reduced dendritic branching and soma shrinkage. (C) Histogram quantifying the reduced number of SMI32-positive α-RGCs at 10 weeks after initial microbead injection compared to control values. (D) Histogram comparing the mean soma size of α-RGCs in normal and glaucomatous retinas. (E, F) Histograms quantifying the reduced dendritic length and perimeter of the dendritic fields of α-RGCs in glaucomatous retinas as compared to controls. For all histograms, $n = 3$ control retinas and $n = 4$ retinas in microbead-injected eyes. Projection of seven images, z = 1-µm steps for panels A and B. Data are presented as mean ± SEM. *$P < 0.05$, ***$P < 0.001$.

arborization followed by shrinkage of the cell soma, which ultimately leads to cell death.[39,40] We therefore examined morphologic alterations of surviving RGCs in glaucomatous retinas at 10 weeks after the initial microbead injection. Whole-mount retinas from control and glaucomatous eyes were double immunostained for Brn3a and for the nonphosphorylated neurofilament marker SMI32, which has been used to label somas, axons, and dendrites of α-RGCs in cats and rodents.[41–43] Although we are not aware which cell type in the marmoset is the homologue of α-RGCs, the SMI32-positive cells we observed had similar features, including large somata, 18 ± 0.6 µm in diameter, long and thick primary dendrites, predominant location in the peripheral retina, and a low 4% to 5% proportion of the entire RGC population (Fig. 3A). At 10 weeks after the initial microbead injection, the number of SMI32-positive RGCs was reduced by ~27% ($P < 0.05$, $n = 3$ eyes) (Figs. 3B, 3C). Furthermore, the surviving SMI32-positive cells exhibited a ~18% shrinkage in soma diameter ($P < 0.001$, $n = 40$–50 cells/eye for three eyes) (Fig. 3D). This was coupled with significant remodeling of their dendritic arbors as indicated by an approximate 50% reduction in dendritic length

and perimeter ($P < 0.001$ for each parameter, $n = 15$–20 cells/eye for three eyes) (Figs. 3E, 3F).

SD-OCT Imaging

SD-OCT imaging was carried out to assess changes in microbead-injected marmoset with similarities to those found in human patients with glaucoma. An enlargement of optic nerve head cupping is often associated with glaucoma.[44] We found that at 10 weeks after microbead injection, treated marmoset eyes exhibited enlarged optic nerve cupping. The eye presented in Figure 4 showed a 0.4 cup-to-disc ratio (c/d ratio) before microbead injection (Fig. 4A) and a 0.95 c/d ratio postinjection (Fig. 4B). All four microbead-injected eyes in the study exhibited optic nerve cupping after treatment. On average, the cup increased from 0.42 (c/d ratio) prior to microbead injection (range, 0.25–0.64) to 0.72 (range, 0.59–0.95) at 10 weeks after the initial microbead injection ($P < 0.05$, $n = 4$ eyes).

Automated segmentation of the SD-OCT scans revealed a significant thinning of the RNFL in marmoset eyes at 10 weeks after the initial microbead injection as compared to control values measured prior to the injection and IOP elevation (week 0) in the superior and nasal paracentral retina (Fig. 4C). The automated segmentation of the SD-OCT scans showed a significant RNFL thinning in glaucomatous marmosets at the end of treatment compared to baseline in the inferior (week 0: 33.73 ± 2.84 µm; week 10: 15.81 ± 0.96 µm), superior (week 0: 33.71 ± 2.41 µm; week 10: 18.07 ± 2.36 µm), and nasal paracentral (week 0: 33.50 ± 0.96 µm; week 10: 27.38 ± 4.35 µm) retinal quadrants ($P < 0.05$, $n = 4$ eyes). In contrast, we found that the RNFL in control retinas showed a modest thickening over the same 10-week experimental period. This supports the idea that the RNFL thinning in microbead-injected eyes was a reflection of cell loss

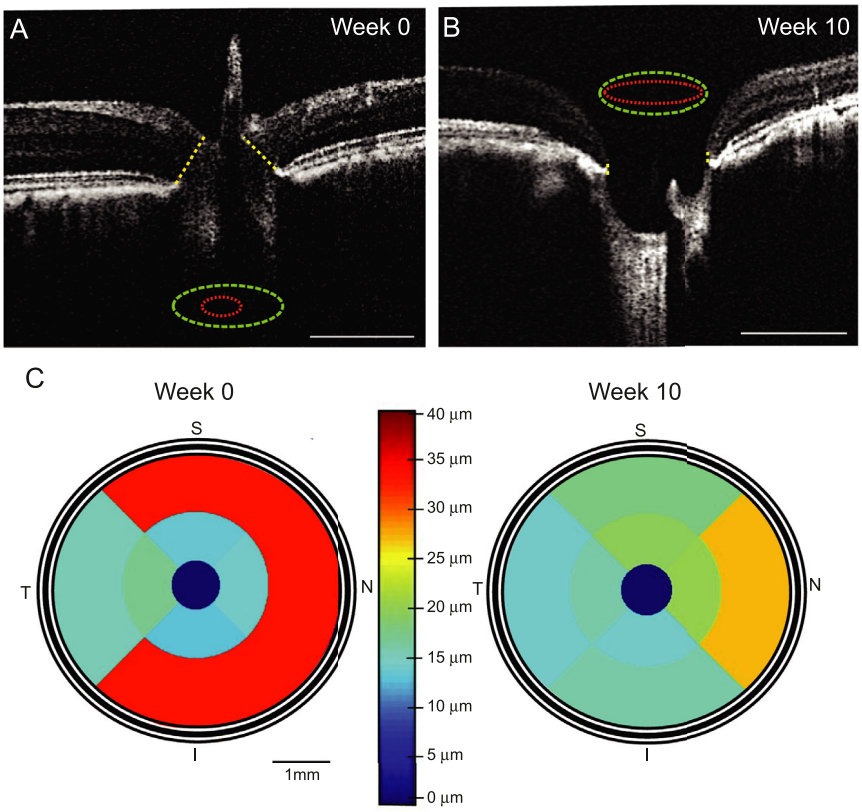

Figure 4. Microbead-injected marmoset eyes show expanded cupping of the optic nerve head and RNFL thinning characteristic of glaucoma. Representative cross-sectional OCT scan from a marmoset before (A) and 10 weeks after (B) intracameral injection of microbeads. The *green outer ring* and *red inner ring* represent the optic nerve head and cup, respectively. The cup was manually identified as the area within the minimum distance between BMO and the internal limiting membrane (BMO–minimum rim width) (*yellow straight dotted lines*). *Scale bar*: 1 mm. (C) Schematic color maps summarizing the average RNFL change occurring from baseline (week 0) to the end of treatment in glaucomatous eyes using the Iowa Reference Algorithms and plotted as color maps using MATLAB (MathWorks).

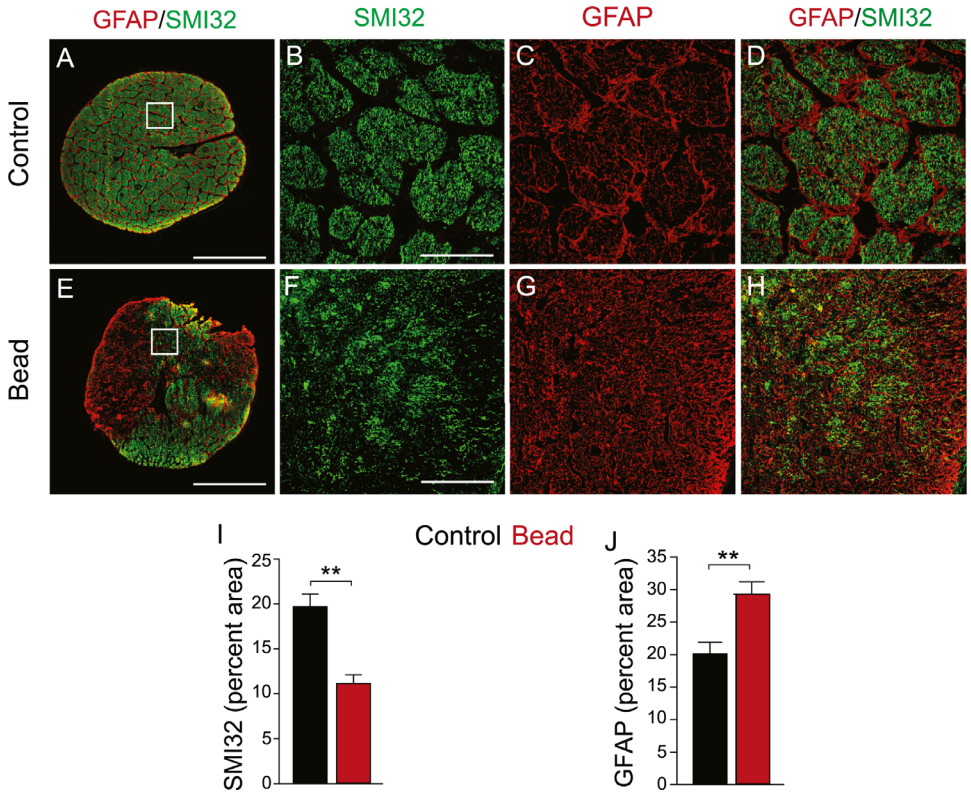

Figure 5. Effects of elevated IOP on optic nerve morphology. (A–D) Representative cross-sectional images of the lamina cribrosa region of the optic nerve from control animals immunostained for SMI32 and GFAP to visualize axonal and astrocytic structure, respectively. Rectangle in panel A shows area of higher magnification in panels B–D. *Scale bars*: 100 µm for panel A and 25 µm for panels B–D. (E–H) Representative cross-sectional images of the lamina cribosa region of the optic nerve from animals 10 weeks after initial microbead injection. A marked disruption of the SMI32-labeled axonal bundles and the honeycomb pattern of GFAP astrocytes are evident. Conventions are the same as in A–D. (I) Histogram quantifying SMI32 labeling in the cross sections of the optic nerves of marmoset under control and glaucomatous conditions ($n = 3$ control eyes and $n = 4$ microbead-injected eyes). (J) Histogram quantifying GFAP labeling in cross sections of optic nerves under control and glaucomatous conditions ($n = 3$ control eyes and $n = 4$ microbead-injected eyes). Projection of five images, z = 1-µm steps for all images. Data are presented as mean ± SEM. $^{**}P < 0.05$.

rather than any natural stretching of the retina over the time course, consistent with our findings of RGC loss presented above.

Optic Nerve Changes in Microbead-Injected Eyes

We next determined the structural changes in the optic nerve in microbead-injected eyes. Cross sections, 8 to 10 µm thick, were obtained at the level of the lamina cribrosa and were double immunolabeled with anti-SMI32 to label RGC axons and anti-GFAP to evaluate axonal loss and astrocytic activity. It has been demonstrated that the degree of optic nerve injury assessed by SMI32 labeling is comparable to that measured by grading of toluidine blue–stained sections, and so it has been routinely employed for detecting axonal swelling and loss in animal models of glaucoma.[45,46] In control eyes, the lamina cribrosa showed a well-organized structure of axonal bundles and surrounding astrocytes forming a characteristic honeycomb mosaic (Figs. 5A, 5B, 5C, 5D). However, at 10 weeks after initial microbead injection, we found significant changes in the structure of the optic nerve, most evidenced by the disruption of the honeycomb mosaic (Figs. 5E, 5F, 5G, 5H). There was a ~45% loss of SMI32-positive axons ($P < 0.01$, $n = 4$ eyes) resulting in a disorganization of the axonal bundles (Figs. 5F, 5I). Astrogliosis was evidenced by a ~40% increase in GFAP expression ($P < 0.01$, $n = 4$ eyes), with glial processes now more disorganized with a shorter and thicker appearance then in control eyes (Figs. 5G, 5J). These structural alterations were consistently observed in the optic nerves of all four glaucomatous eyes tested.

Discussion

The use of animal models has been long established as a useful paradigm to determine the pathogenesis of human glaucoma, thereby providing insights into the design of effective treatments. Most studies have focused on mouse models due to their low cost, short breeding cycles, and accessibility to genome manipulation. However, to determine if rodent data are useful for understanding the human condition, an important next step is to recapitulate these findings in NHP glaucoma models.[7,11] Indeed, a number of NHP models of glaucoma have been created, but some have been plagued by difficult experimental manipulations that lead to variable results as well as the high cost of colony maintenance. The marmoset microbead occlusion model of glaucoma we demonstrated here used a relatively simple technique that produced consistent elevations of IOP for at least 10 weeks, which we chose as our experimental period. Moreover, the marmoset has several advantages over other NHPs as they are relatively small and easy to handle, breed well in captivity, are cost effective, and have been shown amenable to genetic manipulations.

Most important, the microbead occlusion marmoset model showed a number of phenotypic changes established as prototypic for both animal and human glaucoma. At 10 weeks after the initial microbead injection, we observed significant death of RGCs at all eccentricities and all four retinal quadrants. There was territoriality to the RGC loss, with the most severe loss of 60% in the peripheral retina, followed by a 47% reduction within the mid-periphery and a central loss of 31%. Regionalized RGC axonal loss has been reported in a DBA/2J mouse model of hereditary glaucoma.[47,48] Furthermore, preferential loss of RGCs in peripheral retina has been described in experimental glaucoma in both NHPs and rodents, consistent with the early loss of peripheral vision in humans.[49–52] Consistent with the RGC loss, we also observed a thinning of the RNFL at 10 weeks after initial microbead injection.

Analyses of RGC morphology in NHP and rodent glaucoma models indicate that dendritic remodeling and somatic shrinkage precede cell death.[39,40,53] Consistent with this idea, we found that surviving SMI32-positive RGCs in glaucomatous retinas exhibited somatic shrinkage and marked dendritic atrophy. Interestingly, within the 10-week time frame, these cells exhibited lower susceptibility to glaucomatous insult, as their loss of ~27% was significantly less than the average 60% loss across the entire RGC population within peripheral retina. These data suggest that RGC subtypes may show a range of susceptibility to glaucomatous damage.

In addition to the RGC loss, we found a significant gliosis in the retina at 10 weeks after the induction of elevated IOP. This was evidenced as a 4- to 5-fold increase in GFAP expression within the central, mid-peripheral, and peripheral regions. These findings suggest extensive homeostatic dysfunction in glaucomatous retinas, which likely contribute to the cellular loss and axonal damage.

The morphologic changes were accompanied by functional changes as evaluated by abnormalities in the photopic flash ERG waveforms. These included a significant reduction in the amplitude of the PhNR, consistent with inner retina damage. The late reductions observed in both a- and b-wave amplitudes are interesting as they suggest subsequent outer retina damage. Consistent with this idea, changes in photoreceptor and bipolar cell structure, as well as their synaptic components, have been reported in glaucomatous retinas.[54,55]

Finally, we observed clear abnormalities in the optic nerve of glaucomatous marmoset eyes. These included an enlarged cupping of the optic nerve head as well as histologic changes at the lamina cribrosa closely resembling those described in human patients and animal models.[9,10,19,45] Astrocytes and microglia play an important role in supporting the structural integrity of the optic nerve and optic nerve head, and it has been posited that glial cells are involved in the pathogenesis of glaucoma, specifically by initiating damage in the optic nerve.[56–58] In the optic nerve of control eyes, we observed a highly organized honeycomb pattern of GFAP-labeled astrocytes that formed glial tubes enclosing axon bundles, presumably providing structural support for the RGC axons. In contrast, the optic nerves of glaucomatous eyes showed a marked disruption of the astrocytic matrix, which was accompanied by significant elevation of gliosis and axonal loss. A similar astrocytic disorganization has been reported in rodent models of glaucoma.[19,45,48]

In conclusion, our data indicate that the microbead occlusion model of the marmoset shows many of the structural and functional abnormalities in the retina and optic nerve typically associated with glaucoma. The advantages of the marmoset, including ease of handling and colony maintenance, together with the facility of the methodology and the 10-week experimental period, make this a robust and rigorous NHP model for studying the pathogenesis and resultant treatment options for glaucoma. While the current study was limited to young adult marmosets, future studies should examine older animals to determine

further similarities to the aging human population most associated with glaucoma. Finally, a future examination of aqueous production and outflow, as described for the owl monkey,[59] will further leverage the marmoset as a preferred NHP model for testing glaucoma therapies.

Acknowledgments

Supported by NIH grants EY026024 and EY007360 and a Shaffer Grant from the Glaucoma Research Foundation awarded to SAB.

Disclosure: **S. Kumar**, None; **A. Benavente-Perez,** None; **R. Ablordeppey,** None; **C. Lin,** None; **S. Viswanathan,** None; **A. Akopian,** None; **S.A. Bloomfield,** Patent application, Research Foundation of the State University of New York (P), Connexin Therapeutics (I)

References

1. Quigley HA. Neuronal death in glaucoma. *Prog Retin Eye Res*.1999;18(1):39–57.
2. Almasieh M, Levin LA. Neuroprotection in glaucoma: animal models and clinical trials. *Annu Rev Vis Sci*. 2017;3:91–120.
3. Bouhenni RA, Dunmire J, Sewell A, et al. Animal models of glaucoma. *J Biomed Biotechnol*. 2012;2012:692609.
4. Chen L, Zhao Y, Zhang H. Comparative anatomy of the trabecular meshwork, the optic nerve head and the inner retina in rodent and primate models used for glaucoma research. *Vision*. 2017;1(1):4.
5. Van Zyl T, Yan W, McAdams A, et al. Cell atlas of aqueous humor outflow pathways in eyes of humans and four model species provides insight into glaucoma pathogenesis. *Proc Natl Acad Sci USA*. 2020;117(19):10339–10349.
6. Rasmussen CA, Kaufman PL. Primate glaucoma models. *J Glaucoma*. 2005;14(4):311–314.
7. Burgoyne CF. The non-human primate experimental glaucoma model. *Exp Eye Res*. 2015;141:57–73.
8. Gaasterland D, Kupfer C. Experimental glaucoma in the rhesus monkey. *Invest Ophthalmol Vis Sci*. 1974;13(6):455–457.
9. Quigley HA, Hohman RM. Laser energy levels for trabecular meshwork damage in the primate eye. *Invest Ophthalmol Vis Sci*. 1983;24(9):1305–1307.
10. Shimazawa M, Nakamura S, Miwa M, et al. Establishment of the ocular hypertension model using the common marmoset. *Exp Eye Res*. 2013;111:1–8.
11. Gardiner SK, Fortune B, Wang L, Downs JC, Burgoyne CF. Intraocular pressure magnitude and variability as predictors of rates of structural change in non-human primate experimental glaucoma. *Exp Eye Res*. 2012;103:1–8.
12. Fedorchak MV, Conner IP, Medina CA, Wingard JB, Schuman JS, Little SR. 28-day intraocular pressure reduction with a single dose of brimonidine tartrate-loaded microspheres. *Exp Eye Res*. 2014;125:210–216.
13. Morrison JC, Moore CG, Deppmeier LM, Gold BG, Meshul CK, Johnson EC. A rat model of chronic pressure-induced optic nerve damage. *Exp Eye Res*. 1997;64(1):85–96.
14. Weber AJ, Zelenak D. Experimental glaucoma in the primate induced by latex microspheres. *J Neurosci Methods*. 2001;111(1):39–48.
15. Morgan JE, Tribble JR. Microbead models in glaucoma. *Exp Eye Res*. 2015;141:9–14.
16. Lambert WS, Carlson BJ, Ghose P, Vest VD, Yao V, Calkins DJ. Towards a microbead occlusion model of glaucoma for a non-human primate. *Sci Rep*. 2019;9(1):1–15.
17. Chan ASY, Tun TA, Allen JC, et al. Longitudinal assessment of optic nerve head changes using optical coherence tomography in a primate microbead model of ocular hypertension. *Sci Reports*. 2020;10(1):14709–14718.
18. Sappington RM, Carlson BJ, Crish SD, Calkins DJ. The microbead occlusion model: a paradigm for induced ocular hypertension in rats and mice. *Invest Ophthalmol Vis Sci*. 2010;51(1):207–216.
19. Akopian A, Kumar S, Ramakrishnan H, Roy K, Viswanathan S, Bloomfield SA. Targeting neuronal gap junctions in mouse retina offers neuroprotection in glaucoma. *J Clin Invest*. 2017;127(7):2647–2661.
20. Sasaki E, Suemizu H, Shimada A, et al. Generation of transgenic non-human primates with germline transmission. *Nature*. 2009;459(7246):523–527.
21. Solomon SG, Rosa MG. A simpler primate brain: the visual system of the marmoset monkey. *Front Neural Circuits*. 2014;8:96.
22. Okano H, Sasaki E, Yamamori T, et al. Brain/MINDS: a Japanese national brain project for marmoset neuroscience. *Neuron*. 2016;92(3):582–590.

23. Agarwal R, Agarwal P. Rodent models of glaucoma and their applicability for drug discovery. *Expert Opin Drug Discov*. 2017;12(3):261–270.
24. Feng H, Zhu X, Nour A, Nieu R, Benavente-Perez A. Changes in macular retinal thickness during emmetropization and myopia development in juvenile marmosets. *Invest Ophthalmol Vis Sci*. 2017;58(8):4433.
25. Ablordeppey RK, Pope A, Zhu X, Benavente-Perez A. Growth-related changes in thickness in the individual retinal layers of marmoset eyes. Paper presented at: Association for Research in Vision and Ophthalmology Annual Meeting (ARVO), May 2, 2019, ARVO meeting in Vancouver, Canada; 2019.
26. Chauhan BC, O'Leary N, AlMobarak FA, et al. Enhanced detection of open-angle glaucoma with an anatomically accurate optical coherence tomography-derived neuroretinal rim parameter. *Ophthalmology*. 2013;120(3):535–543.
27. Troilo D, Howland HC, Judge SJ. Visual optics and retinal cone topography in the common marmoset (*Callithrix jacchus*). *Vision Res*. 1993;33(10):1301–1310.
28. Wilder HD, Grunert U, Lee BB, Martin PR. Topography of ganglion cells and photoreceptors in the retina of a New World monkey: the marmoset *Callithrix jacchus*. *Vis Neurosci*. 1996;13(2):335–352.
29. Viswanathan S, Frishman LJ, Robson JG, Harwerth RS, Smith EL. The photopic negative response of the macaque electroretinogram: reduction by experimental glaucoma. *Invest Ophthalmol Vis Sci*. 1999;40(6):1124–1136.
30. Viswanathan S, Frishman LJ, Robson JG, Walters JW. The photopic negative response of the flash electroretinogram in primary open angle glaucoma. *Invest Ophthalmol Vis Sci*. 2001;42(2):514–522.
31. Bush RA, Sieving PA. A proximal retinal component in the primate photopic ERG a-wave. *Invest Ophthalmol Vis Sci*. 1994;35(2):635–645.
32. Sieving PA, Murayama K, Naarendorp F. Push-pull model of the primate photopic electroretinogram: a role for hyperpolarizing neurons in shaping the b-wave. *Vis Neurosci*. 1994;11(3):519–532.
33. Fernández-Sánchez L, De Sevilla Müller LP, Brecha NC, Cuenca N. Loss of outer retinal neurons and circuitry alterations in the DBA/2J mouse. *Invest Ophthalmol Vis Sci*. 2014;55(9):6059–6072.
34. Ortín-Martínez A, Salinas-Navarro M, Nadal-Nicolás FM, et al. Laser-induced ocular hypertension in adult rats does not affect non-RGC neurons in the ganglion cell layer but results in protracted severe loss of cone-photoreceptors. *Exp Eye Res*. 2015;132:17–33.
35. Kumar S, Ramakrishnan H, Viswanathan S, Akopian A, Bloomfield SA. Neuroprotection of the inner retina also prevents secondary outer retinal pathology in a mouse model of glaucoma. *Invest Ophthalmol Vis Sci*. 2021;62(9):35.
36. Inman DM, Horner PJ. Reactive nonproliferative gliosis predominates in a chronic mouse model of glaucoma. *Glia*. 2007;55(9):942–953.
37. Nadal-Nicolás FM, Jiménez-López M, Sobrado-Calvo P, et al. Brn3a as a marker of retinal ganglion cells: qualitative and quantitative time course studies in naive and optic nerve-injured retinas. *Invest Ophthalmol Vis Sci*. 2009;50(8):3860–3868.
38. Gomes FL, Silveira LC, Saito CA, Yamada ES. Density, proportion, and dendritic coverage of retinal ganglion cells of the common marmoset (*Callithrix jacchus jacchus*). *Braz J Med Biol Res*. 2005;38(6):915–924.
39. Weber AJ, Kaufman PL, Hubbard WC. Morphology of single ganglion cells in the glaucomatous primate retina. *Invest Ophthalmol Vis Sci*. 1998;39(12):2304–2320.
40. El-Danaf RN, Huberman AD. Characteristic patterns of dendritic remodeling in early-stage glaucoma: evidence from genetically identified retinal ganglion cell types. *J Neurosci*. 2015;35(6):2329–2343.
41. Cleland BG, Levick WR, Wässle H. Physiological identification of a morphological class of cat retinal ganglion cells. *J Physiol*. 1975;248(1):151–171.
42. Peichl L, Ott H, Boycott BB. Alpha ganglion cells in mammalian retinae. *Proc R Soc Lond B Biol Sci*. 1987;231(1263):169–197.
43. Sanes JR, Masland RH. The types of retinal ganglion cells: current status and implications for neuronal classification. *Annu Rev Neurosci*. 2015;38:221–246.
44. Burgoyne CF, Downs JC, Bellezza AJ, Suh JK, Hart RT. The optic nerve head as a biomechanical structure: a new paradigm for understanding the role of IOP-related stress and strain in the pathophysiology of glaucomatous optic nerve head damage. *Prog Retin Eye Res*. 2005;24(1):39–73.
45. Sun D, Lye-Barthel M, Masland RH, Jakobs TC. The morphology and spatial arrangement of astrocytes in the optic nerve head of the mouse. *J Comp Neurol*. 2009;516(1):1–19.
46. Renner M, Stute G, Alzureiqi M, et al. Optic nerve degeneration after retinal ischemia/reperfusion in

a rodent model. *Front Cell Neurosci*. 2017;11: 254.
47. Schlamp CL, Li Y, Dietz JA, Janssen KT, Nickells RW. Progressive ganglion cell loss and optic nerve degeneration in DBA/2J mice is variable and asymmetric. *BMC Neurosci*. 2006;7(1):1–14.
48. Howell GR, Libby RT, Jakobs TC, et al. Axons of retinal ganglion cells are insulted in the optic nerve early in DBA/2J glaucoma. *J Cell Biol*. 2007;179(7):1523–1537.
49. Glovinsky Y, Quigley HA, Dunkelberger GR. Retinal ganglion cell loss is size dependent in experimental glaucoma. *Invest Ophthalmol Vis Sci*. 1991;32(3):484–491.
50. Holcombe DJ, Lengefeld N, Gole GA, Barnett NL. Selective inner retinal dysfunction precedes ganglion cell loss in a mouse glaucoma model. *Br J Ophthalmol*. 2008;92(5):683–688.
51. Weinreb RN, Aung T, Medeiros FA. The pathophysiology and treatment of glaucoma: a review. *JAMA*. 2014;311(18):1901–1911.
52. Odden JL, Mihailovic A, Boland MV, Friedman DS, West SK, Ramulu PY. Evaluation of central and peripheral visual field concordance in glaucoma. *Invest Ophthalmol Vis Sci*. 2016;57(6):2797–2804.
53. Morgan JE, Uchida H, Caprioli J. Retinal ganglion cell death in experimental glaucoma. *Br J Ophthalmol*. 2000;84:303–310.
54. Cuenca N, Pinilla I, Fernández-Sánchez L, et al. Changes in the inner and outer retinal layers after acute increase of the intraocular pressure in adult albino Swiss mice. *Exp Eye Res*. 2010;91(2):273–285.
55. Choi SS, Zawadzki RJ, Lim MC, et al. Evidence of outer retinal changes in glaucoma patients as revealed by ultrahigh-resolution in vivo retinal imaging. *Br J Ophthalmol*. 2011;95(1):131–141.
56. Morgan JE. Optic nerve head structure in glaucoma: astrocytes as mediators of axonal damage. *Eye (Lond)*. 2000;14(3):437–444.
57. Williams PA, Marsh-Armstrong N, Howell GR. Lasker /IRRF initiative on astrocytes and glaucomatous neuroinflammation in glaucoma: a new opportunity. *Exp Eye Res*. 2017;157:20–27.
58. Hernandez MR. The optic nerve head in glaucoma: role of astrocytes in tissue remodeling. *Prog Retin Eye Res*. 2000;19(3):297–321.
59. Bartels S. Aqueous humor flow measured with fluorophotometry in timolol-treated primates. *Invest Ophthal Vis Sci*. 1988;29(10):1498–1504.